# Key Parameters for the Synthesis of Active and Selective Nanostructured 3d Metal Catalysts Starting from Coordination Compounds – Case Study: Nickel Mediated Reductive Amination

Mara Klarner,[a] Patricia Blach,[b, c] Haiko Wittkämper,[d] Niels de Jonge,[b, c] Christian Papp,[d] and Rhett Kempe*[a]

The design of nanostructured catalysts based on earth-abundant metals that mediate important reactions efficiently, selectively and with a broad scope is highly desirable. Unfortunately, the synthesis of such catalysts is poorly understood. We report here on highly active Ni catalysts for the reductive amination of ketones by ammonia employing hydrogen as a reducing agent. The key functions of the Ni-salen precursor complex during catalyst synthesis have been identified: (1) Ni-salen complexes sublime during catalyst synthesis, which allows molecular dispersion of the metal precursor on the support material. (2) The salen ligand forms a nitrogen-doped carbon shell by decomposition, which embeds and stabilizes the Ni nanoparticles on the $\gamma$-Al$_2$O$_3$ support. (3) Parameters, such as flow rate of the pyrolysis gas, determine the carbon supply for the embedding process of Ni nanoparticles.

## Introduction

Reductive amination is a very important reaction because the products, alkyl amines, are used intensively as fine and bulk chemicals, pharmaceuticals, and agrochemicals.[1] More specifically, primary amines are the starting material for the production of other amines or N-heterocyclic compounds.[2] The synthesis of primary amines via reductive amination is very challenging, because overalkylation and other side reactions must be avoided. The reductive amination for the synthesis of primary amines with hydrogen as a reducing agent was introduced 100 years ago by Mignonac, employing a Ni catalyst.[3] The use of hydrogen as a potentially sustainable and cost-effective reductant is particularly attractive, however, a

catalyst is required for its activation. Furthermore, inexpensive ammonia is utilized as a nitrogen source. Despite the use of Ni catalysts ever since,[4,5] no catalyst system for the synthesis of primary amines with a broad scope and functional group tolerance had been found until 2019. We then presented a nanostructured Ni catalyst for the synthesis of primary amines by reductive amination, using ammonia dissolved in water.[5] Our catalyst had a broad scope and an exceptional tolerance towards functional groups, operated at low temperature and pressure, was highly active, reusable, and easy to handle. The synthesis from a specific Ni complex, namely, a Ni-salen complex, and $\gamma$-Al$_2$O$_3$ was straightforward, and the ligand-metal combination of this complex was crucial. Other interesting earth-abundant metal catalysts, synthesized via the pyrolysis of salen complexes, were reported by us[6] and the Beller group.[7,8] The superior performance of catalyst systems based on salen precursor complexes was demonstrated in all these publications. Unfortunately, the role of salen complexes in the pyrolysis-based catalyst synthesis is incompletely understood.

Herein, we report on a highly active Ni catalyst for the reductive amination of ketones by ammonia employing hydrogen as reductant. This Ni/Al$_2$O$_3$ catalyst was obtained by varying the nickel salen complex precursors used for the catalyst synthesis. Thereby, the key functions of the Ni-salen precursor complex during catalyst synthesis have been identified: (1) The volatility of Ni-salen complexes allows the molecular dispersion of the metal precursor on the support material, which enables an optimal bottom-up approach for the preparation of catalytically active metal sites. (2) Tailored decomposition of the carbon and nitrogen containing salen ligand forms a nitrogen-doped carbon shell that covers the catalytically active nickel nanoparticles, thereby stabilizing them. (3) A specific set of parameters during the pyrolysis step in catalyst generation determines the carbon supply, which is crucial for the embedding process

[a]  M. Klarner, Prof. R. Kempe
     Anorganische Chemie II – Catalyst Design,
     Sustainable Chemistry Centre
     University of Bayreuth
     Universitätsstraße 30, 95440 Bayreuth (Germany)
     E-mail: kempe@uni-bayreuth.de
[b]  P. Blach, Prof. N. de Jonge
     INM – Leibniz Institute for New Materials
     Campus D2 2, 66123 Saarbrücken (Germany)
[c]  P. Blach, Prof. N. de Jonge
     Department of Physics
     Saarland University
     Campus D2 2, 66123 Saarbrücken (Germany)
[d]  H. Wittkämper, Dr. C. Papp
     Physical Chemistry II
     Department of Chemistry and Pharmacy,
     University Erlangen-Nürnberg
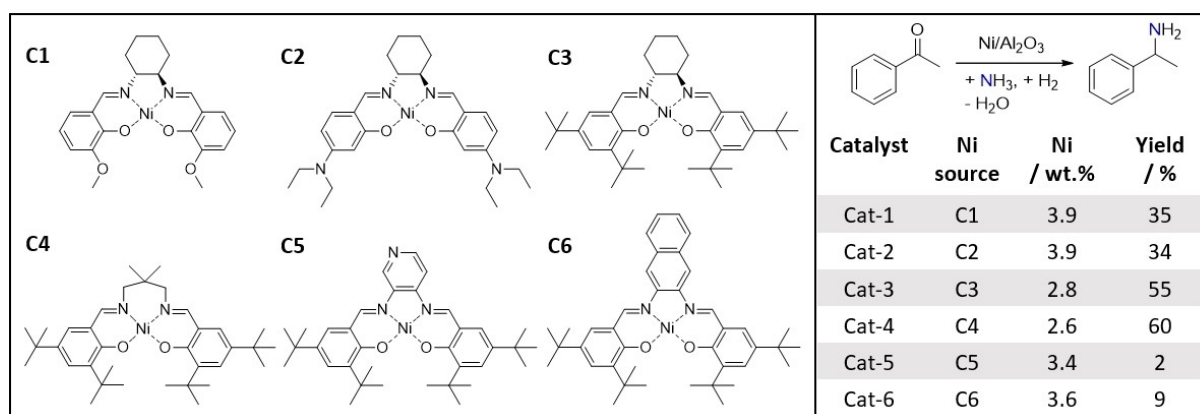     91058 Erlangen (Germany)

of nanoparticles. A too high carbon supply particularly favors the undesired formation of carbon nanotubes.

## Results and Discussion

We developed a Ni complex library to better address the question about the role and the mandatory nature of Ni-salen complexes in the generation of highly active hydrogenation catalysts. Based on this, alumina-supported catalysts were prepared and investigated for their catalytic activity in the reductive amination of acetophenone as a model reaction. The Ni-salen ligand structures were selected by fine-tuning the steric properties and carbon and nitrogen content by choosing appropriate amine precursors and ring substituents. Starting from the known Ni precursor C1[5] three different aldehydes and four different diamines, including aliphatic, N-heteroaromatic und polyaromatic compounds, were combined. A total of six complexes, C1 to C6, were synthesized, as outlined in Figure 1. The corresponding $Ni/Al_2O_3$ composite catalysts Cat-1 to Cat-6 were generated along an established three-step protocol for 3d metal catalysts supported on commercial supports[5,6]: The γ-$Al_2O_3$ support was wet impregnated with C1 to C6 (ideally 4 wt.% nickel) in acetonitrile. After removal of the solvent, the samples were pyrolyzed in a nitrogen flow up to 700 °C, followed by a reduction step in forming gas at 550 °C.

The catalytic activity of the $Ni/Al_2O_3$ catalysts Cat-1 to Cat-6 was compared in the reductive amination of acetophenone as a model reaction. The table in Figure 1 gives an overview of the catalytic activity of the catalysts and the respective loading of nickel nanoparticles. We discovered an obvious dependence of the performance of $Ni/Al_2O_3$ catalysts on the Ni precursor complex used. Cat-4 showed the highest activity with a yield of 60% of 1-phenylethylamine, followed by Cat-3 (55%). By contrast, Cat-5 (2%) and Cat-6 (9%) were nearly inactive in the reductive amination of acetophenone under these reaction conditions. It was shown that the catalytic activity of the $Ni/$

$Al_2O_3$ catalyst published,[5] Cat-1 (35%), was surpassed by fine-tuning the salen ligand, which, similar to Cat-2 (34%), led to only a moderate yield. Salen complexes are known to sublime without decomposition.[9] Consequently, the volatility of the Ni-salen complexes was investigated by thermogravimetric analysis (TGA) analogous to the catalyst preparation parameters (Supporting Information, Figure S1). All Ni salen complexes C1 to C6 volatilize into the gas phase above 400 °C (Supporting Information, Table S1). Intriguingly, the compounds C3 and C4 show significantly higher volatility than the other Ni-salen complexes. Possibly, the attached di-*tert*-butyl substituted aromatic rings and aliphatic backbones are beneficial. Inductively coupled plasma optical emission spectroscopy (ICP-OES) was used to analyze the amount of Ni in the $Ni/Al_2O_3$ catalysts. Depending on the volatility of the Ni-salen complex used, the nickel loading of the $Al_2O_3$ support decreased due to removal in the gas flow during catalyst preparation. Cat-3 and Cat-4 showed the lowest Ni loadings of 2.8 wt.% and 2.6 wt.%, respectively, while less volatile Ni precursors resulted in higher Ni contents (Figure 1). In addition, the carbon and nitrogen contents were determined by elemental analysis, reflecting the atomic composition of the salen precursors (Supporting Information, Table S2, Figure S2). Transmission electron microscopy (TEM) analysis of $Ni/Al_2O_3$ materials (Supporting Information, Figure S3) showed a subordinate dependence of the Ni particle size on the precursor complex. The average Ni particle size of the catalysts varied from 8.0 to 11.0 nm with narrow size distribution. Only Ni salen complex C2 was decomposed to larger Ni particles of 30 nm in diameter. The Ni particle size did not alter due to catalysis, as exemplified for Cat-4 (Supporting Information, Figure S4). Initial results did not give a clear indication that the Ni particle size and/or the amount of nickel, carbon and nitrogen in the $Ni/Al_2O_3$ catalyst is the determining factor for a high catalytic activity. However, we observed a qualitative effect of the precursor complex itself. Since there might be a correlation between the high hydrogenation activity of Cat-4 and the volatility of the Ni-salen complex C4, this led to



| Catalyst | Ni source | Ni / wt.% | Yield / % |
|---|---|---|---|
| Cat-1 | C1 | 3.9 | 35 |
| Cat-2 | C2 | 3.9 | 34 |
| Cat-3 | C3 | 2.8 | 55 |
| Cat-4 | C4 | 2.6 | 60 |
| Cat-5 | C5 | 3.4 | 2 |
| Cat-6 | C6 | 3.6 | 9 |

**Figure 1.** A library concept of 6 Ni-salen complex precursors: Ni-salen complexes C1 to C6 synthesized by fine-tuning the steric properties and carbon and nitrogen content (left). The catalytic activity of $Ni/Al_2O_3$ catalysts Cat-1 to Cat-6 studied in the reductive amination of acetophenone depending on the Ni source (right). In order to ensure comparability, the reaction conditions from Ref. [5] were adjusted so that no complete conversion of the reactant occurred: 1.2 mol% $Ni/Al_2O_3$ catalyst (0.006 mmol Ni, 0.35 mg Ni), 0.5 mmol acetophenone, 0.5 mL aq. $NH_3$ (25%, 6.7 mmol), 2 mL $H_2O$, 80 °C, 0.5 MPa $H_2$, 20 h. Yields were determined by gas chromatography using *n*-dodecane as an internal standard. Ni content was analysed by ICP-OES.

**These are not the final page numbers!** ↗↗

**ChemCatChem**

**Full Papers**
doi.org/10.1002/cctc.202100562

**Chemistry
Europe**
European Chemical
Societies Publishing

the hypothesis that volatility might play a crucial role in the generation of catalytically active metal sites. Therefore, we investigated the role of the Ni-salen complex during active catalyst formation exemplified by complex C4. The following three key properties were identified:
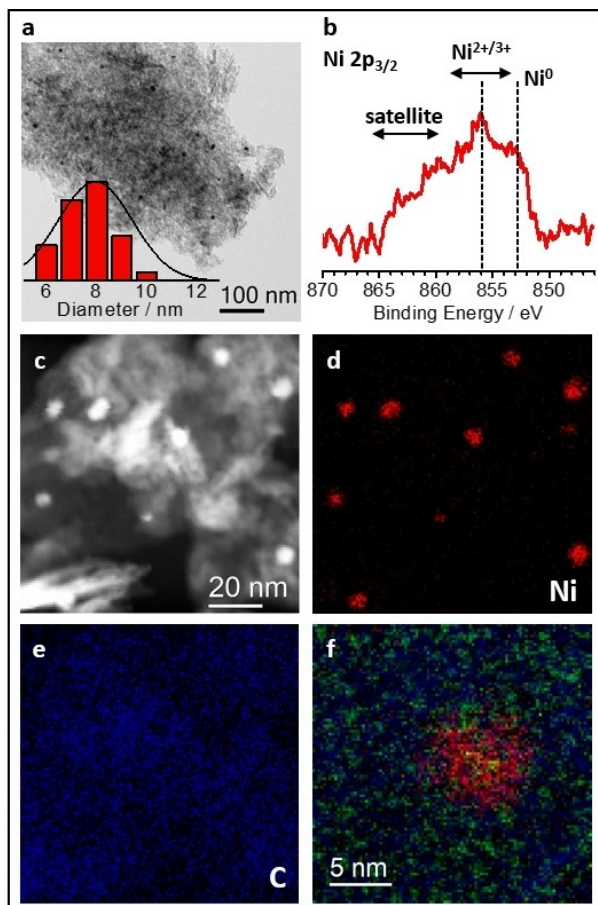
**(1) Molecular Dispersion of the Metal Precursor on the Support Material.** Firstly, we focused on the interaction of the Ni-salen complex C4 with the $Al_2O_3$ support material during the impregnation and pyrolysis steps in catalyst preparation. We found by TEM analysis of wet impregnated $C4/Al_2O_3$ (Supporting Information, Figure S6) that C4 crystallizes in needles several micrometers long, starting from $Al_2O_3$ agglomerates as nucleation centers once the solvent is removed. This method of impregnation does not yield molecular dispersion of C4 on $Al_2O_3$ to produce small Ni nanoparticles directly during pyrolysis. Comparative TGA analysis (Figure 2a) of salen ligand L4, Ni salen complex C4 and impregnated $C4/Al_2O_3$ showed that the salen ligand is already volatile, being thermally stabilized by the chelating coordination of nickel. C4 itself sublimes at a temperature of 469 °C without decomposing, confirmed by
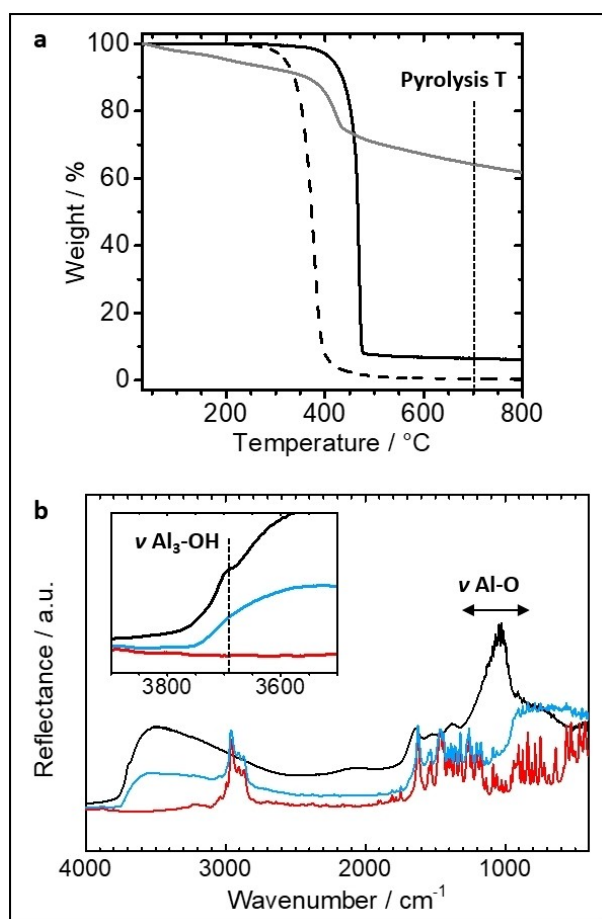


**Figure 2.** (a) TGA analysis (heating ramp 10 K/min, in $N_2$ flow) of L4 (dashed), C4 (black) and impregnated $C4/Al_2O_3$ (grey) demonstrating the volatility of salen compounds. (b) DRIFTS analysis of $Al_2O_3$ (black), C4 (red) and $C4/Al_2O_3$ (blue, heated to $T_{subl}$ 469 °C of C4) confirming the interaction of the Ni-salen complex C4 with the $Al_2O_3$ support. The $Al_3$-OH band is shown in the inset.

mass spectrometry of the residue (Supporting Information, Figure S5). As briefly discussed above, a Ni loading of 2.6 wt.% implies that about 65% of C4 was decomposed on the $Al_2O_3$ support during pyrolysis. Considering the almost quantitative sublimation of the pure C4 (92%), this is a clear indication of an attractive interaction of the Lewis-acidic $Al_2O_3$ surface and the Ni-salen complex. In addition, we investigated the interaction of the Ni-salen complex C4 with the $Al_2O_3$ surface using diffuse reflectance infrared Fourier transform spectroscopy (DRIFTS). As measured in pure $Al_2O_3$, the vibrational band of acidic $Al_3$-OH is centered at 3696 $cm^{-1}$ and the broad signal at 1250–900 $cm^{-1}$ originates from Al-O (Figure 2b).[10] The DRIFTS spectrum shows a very broad band in the hydroxyl spectral region (4000–2500 $cm^{-1}$) since the untreated $Al_2O_3$ sample is surface hydrated by physically absorbed water molecules. The DRIFTS spectrum of Ni-salen complex C4 shows signals in the fingerprint region for wavenumbers lower than 1680 $cm^{-1}$, with the characteristic signal at 1625 $cm^{-1}$ originating from the C=N imine stretching. The bands between 2951 and 2843 $cm^{-1}$ were assigned to C-H stretching vibrations. When impregnated $C4/Al_2O_3$ was heated to 469 °C as during catalyst formation and then cooled to room temperature, the band at 3696 $cm^{-1}$ was no longer visible in the spectrum. The lack of a characteristic $Al_3$-OH band suggests a surface-absorbed complex C4 interacting with acidic centers of $Al_2O_3$. The TEM analysis of this material showed no crystals of C4 (Supporting Information, Figure S6). As exemplified for C4, Ni-salen complexes sublime during $Ni/Al_2O_3$ catalyst generation with negligible decomposition. This property allows the molecular dispersion of single complex molecules on the $Al_2O_3$ surface from the gas phase. Since this dispersion cannot be achieved by wet impregnation with C4, the volatility of the complexes plays a key role in this bottom-up approach to generate catalytically active metal sites.

**(2) Formation of a Nitrogen-doped Carbon Shell for the Stabilization of Nickel Nanoparticles**. We recorded X-ray photoelectron spectroscopy (XPS) survey spectra between 0–1100 eV, given in Figure S7. All expected lines for the $Al_2O_3$ support were identified, and in addition, carbon and minor traces of nitrogen were found. Small Ni signals were detected in the Ni 2p region (Figure 3b), but further Ni lines were not identified due to their small photoemission cross section and their partial overlap with Al lines. The $Ni/Al_2O_3$ catalyst shows a combination of metallic $Ni^0$ signals located at 852.6 eV and a broad signal located at around 854.6 eV which we assigned to oxidized $Ni^{2+}$. Contributions of $Ni^{3+}$ are also possible due to the width of the signal. The 6 eV satellite of Ni is found as a broad feature between 858.6 and 865 eV.[11] The intensity ratio of $Ni^0$: $Ni^{2+}$ is approximately 1.5:2. The C 1s signal observed at 284.7 eV is close to what is typically observed for graphitic carbon.[12] The binding energy of the N 1s signal observed is at around 399.2 eV, possibly a remnant of the N-containing precursor molecule and its decomposition products (Supporting Information, Figure S7). High-angle annular dark-field scanning TEM (HAADF-STEM) analysis of $Ni/Al_2O_3$ confirmed the homogeneous distribution of Ni nanoparticles with an average size of 8.0 nm on the $Al_2O_3$ support material (Figure 3a, c). Energy

**These are not the final page numbers!** ⌐⌐

**ChemCatChem**                    Full Papers
                                   doi.org/10.1002/cctc.202100562

Chemistry
Europe
European Chemical
Societies Publishing

**Figure 3.** Characterization of Ni/Al$_2$O$_3$: (a) TEM image of the Ni/Al$_2$O$_3$ catalyst shows that the Al$_2$O$_3$ support is covered with homogeneously distributed Ni nanoparticles. The size distribution of Ni particles is given in the inset. (b) XPS analysis of the Ni 2p$_{3/2}$ region revealed minor traces of Ni within the composite material. The Ni$^0$ nanoparticles are surface oxidized to Ni$^{2+}$/Ni$^{3+}$ species. (c) HAADF-STEM analysis of the Ni/Al$_2$O$_3$ catalyst and (d, e) representative EDX element maps of nickel (red) and carbon (blue). (f) Overlapped EELS element maps of nickel (red), carbon (blue) and nitrogen (green) demonstrating the embedding of a Ni particle in a N-doped carbon layer.

dispersive X-ray (EDX) elemental maps for nickel and carbon recorded in the same image section illustrate the embedding of Ni nanoparticles in a carbon matrix covering the entire support material (Figure 3d, e). Electron energy loss spectroscopy (EELS) was used to study the near environment of a single nickel nanoparticle. The carbon and the nitrogen component cover the Ni particle and the surrounding support material (Figure 3f). We conclude, from XPS and HAADF-STEM investigations that the decomposition of the salen ligand on γ-Al$_2$O$_3$ during catalyst generation provides a defined N-doped carbon shell that stabilizes the Ni nanoparticles on the support material.

**(3) Determination of the Carbon Supply during the Pyrolysis Step.** Impregnated C4/Al$_2$O$_3$ material was sealed in a quartz glass ampoule in inert atmosphere and treated according to the standard catalyst synthesis process. Carbon nanotubes with a diameter of 30–40 nm grew in this confined gas space, starting from Ni particles of the same size (Supporting Information,
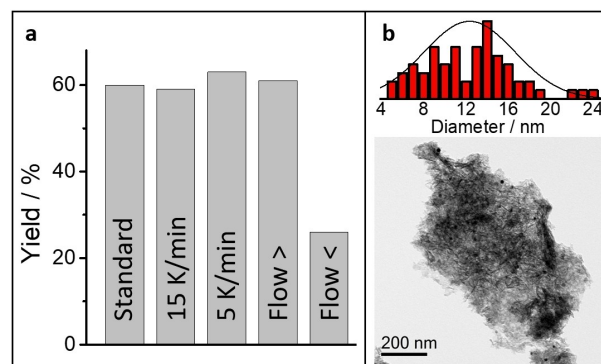


**Figure 4.** (a) The variation of the heating ramp (standard 10 K/min ± 5 K/min) and N$_2$ gas flow (1.25 × and 0.25 × standard flow) during Ni/Al$_2$O$_3$ catalyst synthesis identified the flow as a critical parameter during the pyrolysis step. Reaction conditions: 1.2 mol% Ni/Al$_2$O$_3$ catalyst (0.006 mmol Ni, 0.35 mg Ni), 0.5 mmol acetophenone, 0.5 mL aq. NH$_3$ (25%, 6.7 mmol), 2 mL H$_2$O, 80 °C, 0.5 MPa H$_2$, 20 h. Yields were determined by gas chromatography using n-dodecane as an internal standard. (b) TEM analysis and the size distribution of nickel particles are shown for Ni/Al$_2$O$_3$ synthesized under reduced N$_2$ flow.

Figure S11). The growth of carbon nanotubes initiated by 3d metal particles is well established.[13] We assume that excess carbon, in the form of the salen ligand and its volatile decomposition products, could not be removed due to the absence of a gas flow, thereby favoring the formation of the carbon nanotubes. Thus, the pyrolysis parameters for heating rate and gas flow were varied during the catalyst synthesis. Changing the heating ramp by ± 5 K/min resulted in consistent catalytic activity of the Ni/Al$_2$O$_3$ catalysts, as the sublimation properties of C4 were not significantly different within this chosen range (Supporting Information, Figure S12). By contrast, changing the N$_2$ flow has a major impact on the catalytic activity. Reducing the nitrogen flow by 75% causes the catalytic activity to collapse (Figure 4a), while increasing the gas flow by 25% to the maximum gas flow of the device shows no effect. The TEM analysis of the less active catalyst material (Figure 4b) revealed a broader Ni particle size distribution and a slightly larger mean diameter of 12.5 nm than for the standard Ni/Al$_2$O$_3$ catalyst. The elemental composition of this material also showed higher mass fractions of nickel, carbon, and nitrogen (3.3 wt.% Ni, 8.1 wt.% C, 0.5 wt.% N) compared to Cat-4 (2.6 wt.% Ni, 4.6 wt.% C, 0.3 wt.% N). This led us to conclude that the volatility of the Ni-salen complex in combination with judiciously chosen pyrolysis parameters regulates the carbon supply during catalyst preparation.

## Conclusion

In conclusion, key parameters for the synthesis of active and selective nanostructured 3d metal catalysts starting from a coordination compound were found, which may enable a more rational design of such catalysts in the future.

**These are not the final page numbers!** ↗↗

## Acknowledgements

## Conflict of Interest

The authors declare no conflict of interest.

[1] a) T. Irrgang, R. Kempe, *Chem. Rev.* **2020**, *120*, 9583–9674; b) K. Murugesan, T. Senthamarai, V. G. Chandrashekhar, K. Natte, P. C. J. Kamer, M. Beller, R. V. Jagadeesh, *Chem. Soc. Rev.* **2020**, *49*, 6273–6328; c) O. I. Afanasyev, E. Kuchuk, D. L. Usanov, D. Chusov, *Chem. Rev.* **2019**, *119*, 11857–11911.

[2] K. Weissermel, H.-J. Arpe, *Industrial Organic Chemistry*; Wiley-VCH, Weinheim, **2008**.

[3] G. Mignonac, *Compt. Rend.* **1921**, *172*, 223–226.

[4] a) A. Skita, F. Keil, *Ber. Dtsch. Chem. Ges. B* **1928**, *61B*, 1682–1692; b) C. F. Winans, H. Adkins, *J. Am. Chem. Soc.* **1933**, *55*, 2051–2058; c) C. F. Winans, *J. Am. Chem. Soc.* **1939**, *61*, 3566–3567; d) E. J. Schwoegler, H. Adkins, *J. Am. Chem. Soc.* **1939**, *61*, 3499–3502; e) W. Wayne, H. Adkins, *J. Am. Chem. Soc.* **1940**, *62*, 3314–3316; f) J. C. Robinson, H. R. Snyder, *Org. Synth.* **1943**, *23*, 68; *Org. Synth.* **1955**, *3*, 717; g) B. S. Biggs, W. S. Bishop, *Org. Synth.* **1947**, *27*, 18; *Org. Synth.* **1955**, *3*, 229; h) K. W. Merz, H. Pfäffle, *Arch. Pharm.* **1955**, *288*, 86–100; i) N. Elming, N. Clauson-Kaas, E. P. Anderson, N. Eliasson, B. Thorell, *Acta Chem. Scand.* **1956**, *10*, 1603–1605; j) A. R. Surrey, G. Y. Lesher, *J. Am, Chem.* **1956**, *78*, 2573–2576; k) M. Freifelder, W. D. Smart, G. R. Stone, *J. Org. Chem.* **1962**, *27*, 2209; l) G. Grethe, H. L. Lee, M. Uskoković, A. Brossi, *J. Org. Chem.* **1968**, *33*, 491–494; m) M. A. Popov, N. I. Shuikin, *Bull. Acad. Sci. USSR, Div. Chem. Sci.* **1962**, *11*, 1014–1017; n) K. A. Pollart, R. E. Miller, *J. Org. Chem.* **1962**, *27*, 2392–2394; o) K. Saigo, M. Kai, N. Yonezawa, M. Hasegawa, *Synthesis* **1985**, *2*, 214–216; p) A. S. C. Chan, C.-c. Chen, Y.-c. Lin, *Appl. Catal. A* **1994**, *119*, L1–L5; q) Y. Hirayama, M. Ikunaka, J. Matsumoto, *Org. Process Res. Dev.* **2005**, *9*, 30–38; r) P. Doležal, O. Machalický, M. Pavelek, P. Kubec, K. Hrádková, R. Hrdina, R. Šuláková, *Appl. Catal. A* **2005**, *286*, 202–210; s) N.-T. Le, A. Byun, Y. Han, K.-I. Lee, H. Kim, *Green Sustainable Chem.* **2015**, *5*, 115–127; t) T. Trégner, J. Trejbal, *Chem. Biochem. Eng. Q.* **2018**, *31*, 455–470; u) W. Chen, Y. Sun, J. Du, Z. Si, X. Tang, X. Zheng, L. Lin, S. Liu, T. Lei, *J. Chem. Technol. Biotechnol.* **2018**, *93*, 3028–3034; v) K. Murugesan, M. Beller, R. V. Jagadeesh, *Angew. Chem. Int. Ed.* **2019**, *58*, 5064–5068; *Angew. Chem.* **2019**, *131*, 5118–5122; w) Y. Zhang, H. Yang, Q. Chi, Z. Zhang, *ChemSusChem* **2019**, *12*, 1246–1255; x) M. Manzoli, E. C. Gaudino, G. Cravotto, S. Tabasso, R. B. N. Baig, E. Colacino, R. S. Varma, *ACS Sustainable Chem. Eng.* **2019**, *7*, 5963–5974; y) H. Yuan, J.-P. Li, F. Su, Z. Yan, B. T. Kusema, S. Streiff, Y. Huang, M. Pera-Titus, F. Shi, *ACS Omega* **2019**, *4*, 2510–2516.

[5] G. Hahn, P. Kunnas, N. de Jonge, R. Kempe, *Nat. Catal.* **2019**, *2*, 71–77.

[6] a) T. Schwob, P. Kunnas, N. de Jonge, C. Papp, H.-P. Steinrück, R. Kempe, *Sci. Adv.* **2019**, *5*, eaav3680; b) T. Schwob, M. Ade, R. Kempe, *ChemSusChem* **2019**, *12*, 3013–3017; c) C. Bäumler, C. Bauer, R. Kempe, *ChemSusChem* **2020**, *13*, 3110–3114.

[7] T. Senthamarai, V. G. Chandrashekhar, M. B. Gawande, N. V. Kalevaru, R. Zboril, P. C. J. Kamer, R. V. Jadadeesh, M. Beller, *Chem. Sci.* **2020**, *11*, 2973–2981.

[8] For a calcination-based synthesis of transition metal doped ceria, see: J. S. Elias, M. Risch, L. Giordano, A. N. Mansour, Y. Shao-Horn, *J. Am. Chem. Soc.* **2014**, *136*, 17193–17200.

[9] a) A. Gleizes, M. Julve, N. Kuzmina, A. Alikhanyan, F. Lloret, Malkerovac, J. L. Sanz, F. Senocq, *Eur. J. Inorg. Chem.* **1998**, 1169–1174; b) M. D. M. C. Ribeiro da Silva, J. M. Goncalves, A. L. R. Silva, P. C. F. C. Oliveira, B. Schröder, M. A. V. Ribeiro da Silva, *J. Mol. Catal. A* **2004**, *224*, 207–212.

[10] a) X. Liu, *J. Phys. Chem. C* **2008**, *112*, 5066–5073; b) J. Webber, J. E. Zorzi, C. A. Perottoni, S. M. e Silva, R. C. D. Cruz, *J. Mater. Sci.* **2016**, *51*, 5170–5184.

[11] A. Grosvenor, M. C. Biesinger, R. St C Smart, N. S. McIntyre, *Surface Science* **2006**, *600*, 1771–1779.

[12] R. Blume, D. Rosenthal, J.-P. Tessonnier, H. Li, A. Knop-Gericke, R. Schlögl, *ChemCatChem* **2015**, *7*, 2871–2881.

[13] a) J. Hafner, M. J. Broniowski, B. R. Azamian, P. Nikolaev, A. G. Rinzler, D. T. Colbert, K. A. Smith, R. E. Smalley, *Chem. Phys. Lett.* **1998**, *296*, 195–202; b) S. Helveg, C. López-Cartes, J. Sehested, P. L. Hansen, B. S. Clausen, J. R. Rostrup-Nielsen, F. Abild-Pedersen, J. K. Nørskov, *Nature* **2004**, *427*, 426–429; c) J. A. Rodríguez-Manzo, M. Terrones, H. Terrones, H. W. Kroto, L. Sun, F. Banhart, *Nat. Nanotechnol.* **2007**, *2*, 307–311; d) T. Schmalz, T. Kraus, M. Günthner, C. Liebscher, U. Glatzel, R. Kempe, G. Motz, *Carbon* **2011**, *49*, 3065–3072.

# FULL PAPERS

**Ni-salen precursor + γ-Al$_2$O$_3$**

**Catalyst Synthesis**

(1) Molecular dispersion on support
(2) Formation of N-doped carbon shell
(3) Determination of carbon supply

**Highly active Ni/Al$_2$O$_3$**

10 nm

*M. Klarner, P. Blach, H. Wittkämper, Prof. N. de Jonge, Dr. C. Papp, Prof. R. Kempe\**

1 – 6

**Key Parameters for the Synthesis of Active and Selective Nanostructured 3d Metal Catalysts Starting from Coordination Compounds – Case Study: Nickel Mediated Reductive Amination**
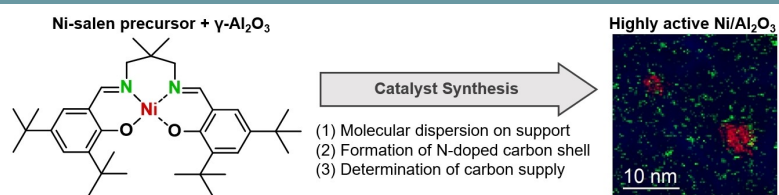
**Reductive Amination:** The Ni/Al$_2$O$_3$ catalyst is highly active in the reductive amination of ketones using ammonia as the nitrogen source and hydrogen as reducing agents. The role of Ni-salen precursor complexes in the catalyst synthesis was identified: Molecular dispersion on the support gives rise to Ni nanoparticles upon decomposition of the complex, which are stabilized by a defined N-doped carbon layer.